Energy Conversion and Management: X 30 (2026) 101624

Contents lists available at ScienceDirect

Energy Conversion and Management: X

journal homepage: www.sciencedirect.com/journal/energy-conversion-and-management-x

# Dual-porosity model for harmonic pulse testing in fractured geothermal reservoir

Peter A. Fokker [a,b], Eloisa Salina Borello [a,*], Francesca Verga [a], Dario Viberti [a]

[a] Politecnico di Torino – DIATI – Corso, Duca degli Abruzzi 24, 10129 Torino, Italy
[b] TNO – Geological Survey of the Netherlands – Princetonlaan 6, 3584 CB Utrecht, the Netherlands

ARTICLE INFO

*Keywords:*
Harmonic pulse testing
Well testing
Geothermal system
Dual-porosity
Frequency analysis

ABSTRACT

Well testing and conventional Pressure Transient Analysis (PTA) are fundamental and well-established methodologies for characterizing well and reservoir parameters. However, the applicability of PTA is limited during production or injection operations, since it requires a shut-in of the tested well, and it is significantly affected by interferences from neighboring wells.

In previous works, we proposed, implemented, and validated against real data a methodology called Harmonic Pulse Testing (HPT). HPT is complementary to PTA. By specifically deploying the periodicity of rate and pressure signals, it has been designed to be applied during ongoing field operations.

In this work, we present a new analytical solution for HPT in naturally fractured reservoirs. The proposed solution is also applied to geothermal systems, as it is coupled with a radial composite model capable of approximating the thermal front. The model has been validated against well-established analytical and numerical models under different scenarios. The calculation steps for converting the numerical dual-porosity model into storativity ratio and inter-porosity flow coefficient are also provided.

The results of a validation exercise demonstrate that our model is robust against potential interference from other wells and allows the detection of the thermal front. The methodology can therefore be successfully applied during ongoing operations in naturally fractured geothermal reservoirs.

## 1. Introduction

Many geothermal reservoirs consist of fractured rock. The bulk of the pore space then is in porous rock blocks, and the bulk of the permeability is in the fractures between the blocks. [1]. In reservoir modeling and Pressure Transient Analysis (PTA), those systems are commonly described by dual-porosity reservoir models [1]. Knowledge and characterization of the flow parameters of such models are crucial for operational planning and economics evaluation, hence the importance of periodic monitoring through a reliable technology and methodology such as well testing. Compared to single-porosity, dual-porosity systems present complications related to pressure dependency of the flow parameters.

Well-testing has traditionally been a powerful method for retrieving the flow and storage properties of subsurface reservoirs [2]. It typically employs injection or production for some time, followed by a shut-in in which the pressure is closely monitored. Analytical or numerical models are then employed to interpret the pressure and rate signals to obtain knowledge about the flow properties. A useful characterization involves the identification of a representative reservoir model and the determination of the model and reservoir parameters. An important tool in well-test analysis is the derivative analysis: the logarithmic time derivative of the pressure change is very sensitive to features like reservoir boundaries, heterogeneities, and fractures, and can therefore be used in a combined visual and algebraic interpretation [3]. The use of time derivatives has been facilitated by the availability of highly sensitive pressure gauges. Shut-in of the active well is usually required to minimize the noise in the pressure measurements.

Well testing procedures have also been developed and employed for dual-porosity systems [4]. A typical feature of pressure transient analysis in dual-porosity media is the valley in the derivative curve that is associated with the activation of the compressible porous volume in the matrix blocks.

However, deploying classical pressure transient analysis has some drawbacks. In the first place, it relies on flow equations for constant

* Corresponding author.
*E-mail addresses:* peter.fokker@tno.nl (P.A. Fokker), eloisa.salinaborello@polito.it (E. Salina Borello), francesca.verga@polito.it (F. Verga), dario.viberti@polito.it (D. Viberti).

https://doi.org/10.1016/j.ecmx.2026.101624
Received 20 May 2025; Received in revised form 25 September 2025; Accepted 22 January 2026
Available online 28 January 2026

**Nomenclature**

| | |
|---|---|
| $C$ | Wellbore storage parameter. $m^3$/Pa |
| $C_D$ | Dimensionless wellbore storage. – |
| $c_f, c_m$ | Total compressibility of fracture system or matrix system. 1/Pa |
| $c_r$ | Rock compressibility. 1/Pa |
| $c_w$ | Water compressibility. 1/Pa |
| $c_t$ | Total compressibility. 1/Pa |
| $I_0, I_1$ | Modified Bessel functions of the first kind. – |
| $K_0, K_1$ | Modified Bessel functions of the second kind. – |
| $k, k_f, k_m$ | Fracture and matrix permeability. $m^2$, md |
| $H$ | Reservoir thickness. m |
| $P, p$ | Fracture pressure and fracture pressure amplitude. Pa |
| $P_m, p_m$ | Matrix pressure and matrix pressure amplitude. Pa |
| $Q_i, q_i$ | Injection rate and injection rate amplitude. $m^3$/s |
| $Q_{loss}, q_{loss}$ | Loss rate from fracture to matrix per unit volume and its amplitude. 1/s |
| $r$ | Radial position. m |
| $r_w$ | Well radius. m |
| $r_{obs}$ | Observation position. m |
| $S$ | Skin. – |
| $t$ | Time. s |
| $\alpha$ | Fracture–matrix geometry factor. $1/m^2$ |
| $\phi_f, \phi_m$ | Porosity of fracture and matrix system with respect to total volume. – |
| $\lambda_1, \lambda_2$ | Fluid mobility in zones 1 and 2. $m^2$/Pa.s |
| $\eta_f, \eta_m$ | Pressure diffusivity constants in fracture and matrix system. $m^2$/s |
| $\zeta, \zeta_f, \zeta_m$ | Bessel function parameter. 1/m |
| $\xi$ | Parameter in unrestricted-flow solution. 1/s |
| $\mu$ | Fluid viscosity. Pa.s |
| $\rho$ | Position in matrix block. m |
| $\rho_m$ | Effective radius of matrix block. m |
| $\omega$ | Angular frequency of pulse test. 1/s |
| $\Lambda$ | Inter-porosity flow coefficient. – |
| $\Omega$ | Storativity ratio. – |

injection or production rates. Tests with non-constant rates can be evaluated with deconvolution techniques, but their application is not always straightforward. Further, high-quality pressure data require well shut-in to remove pressure disturbances originating from the flowing fluids. Even the interference with neighboring wells can distort the signal in such a way that interpretation is hindered, and those may have to be shut in as well. However, well shut-in is potentially very costly as it takes away time for injection and production operations. In addition, measurements during well shut-in naturally target properties at zero flow – while properties in fractured media may be quite dependent on the flow conditions [5].

Pulse testing was originally deployed as an interference testing tool, by applying pulses to one well and measuring the inter-well connectivity through the response in a second well [6]. Later, it was extended to Harmonic Pulse Testing (HPT), in which the pulses are of exactly equal duration [7]. This approach enables evaluation in the frequency domain, after performing a Fourier transformation on the signal. The advantage of analysis in the Fourier domain is the smaller sensitivity to erratic pressure variations, thus facilitating deployment during ongoing operations [8]. Such deployment enables the determination of parameters during production or injection, and it reduces the expensive non-operational time of a well.

Analytical solutions of the diffusivity equation with harmonic boundary conditions are available for several common scenarios. Different solutions incorporating both wellbore storage (C) and skin (S) effects were provided by [7–9]. Solutions can include early-time effects due to the well geometry (partial penetration, horizontal well) [10], as well as late-time effects (i.e., closed boundary, sealing fault) [10] and non-Darcy effects [11]. For the injection of non-isothermal fluid, as is often the case in geothermal energy applications, pulse testing can be deployed to identify the position of the thermal front [12]. However, the presence of fractures complicates the subsurface response. Applying simple radial composite models gives storativity and transmissivity numbers that are dependent on the driving frequency. Such behavior could, for instance, be related to the aperture heterogeneity of the fractured system and the fracture hydromechanics. That very same point has also already been made by [13]. They performed periodic pumping tests in a borehole at the Grimselpass in Switzerland. The fractured system made the hydraulic properties dependent on pressure, complicating the use of superposition models and Fourier analysis. A similar conclusion was reached by [10] when interpreting a pulse test during a hydraulic stimulation in the Pohang enhanced geothermal system [14]. Models with more complexity than simple homogeneous, constant permeability, and compressibility are needed. Numerical solutions for HPT interpretation in presence of heterogeneities [15] or in presence of a complex fracture pattern [16] have also been proposed, but they are poorly suitable for fractured systems because they require an accurate description of the fracture system geometry. Moreover, they involve a significantly higher computational effort.

In the present contribution, we develop an analytical solution in the frequency domain with the hypothesis of a dual-porosity system for both restricted and unrestricted-flow conditions in the matrix blocks.

## 2. Material and methods

### 2.1. Model framework

We consider a well in a 2D radially symmetric fractured reservoir.

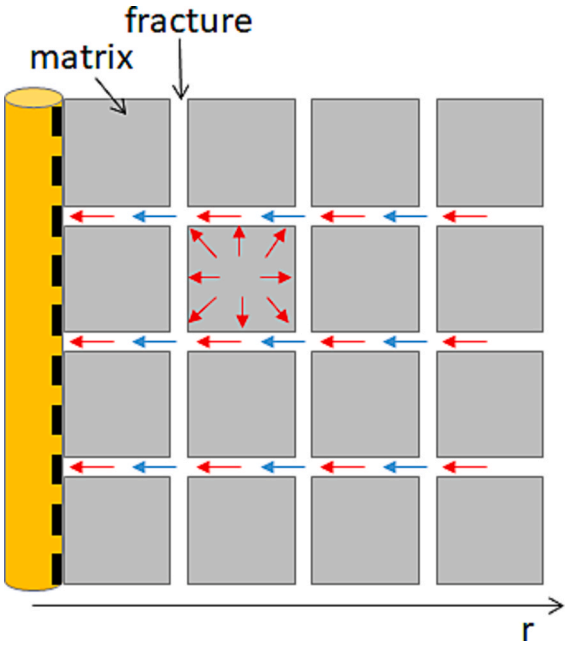


**Fig. 1.** Idealization of the heterogeneous porous medium into the dual–porosity model; fissured system production (blue arrows) vs. total system production (red arrows).

The reservoir is modeled as a dual-porosity system with two overlapping domains (Fig. 1): the matrix and the fracture domain [4]. The system porosity ($\phi$) is the sum of the porosity of the fractured domain ($\phi_f$) and the porosity of the matrix domain ($\phi_m$):

$$\phi = \phi_f + \phi_m \tag{1}$$

where, differently from what is proposed by [3], we define the porosity of both matrix and fracture systems with respect to the total reservoir volume, coherently with the definition of the numerical simulator adopted for validation. If calculated only within the fracture domain, the fracture porosity would approach 1; however, when considered relative to the total reservoir volume, which is predominantly occupied by the matrix, its value is significantly reduced.

Being fracture permeability ($k_f$) significantly higher than matrix permeability ($k_m$), the flow occurs mainly in the fractured domain:

$$kh \approx k_f h_f \tag{2}$$

Similarly to [4], the model is characterized by two dimensionless parameters: the storativity ratio ($\Omega$), and the inter-porosity flow coefficient ($\Lambda$):

$$\Omega = \frac{\phi_f c_f}{\phi_f c_f + \phi_m c_m} \tag{3}$$

$$\Lambda = \alpha r_w^2 \frac{k_m}{k_f} \tag{4}$$

Unlike the conventional notation [4], we use capital Greek letters $\Omega$ and $\Lambda$ to avoid confusion with angular frequency, $\omega$, that will be introduced later, and with the symbol $\lambda$ commonly used for mobility.

The storativity ratio ($\Omega$), eq. (3), quantifies the fraction of fluid storage residing in the fracture system relative to the combined storage of the fracture and matrix systems; it is typically in the range of $0.01 \leq \Omega \leq 0.1$.

The inter-porosity flow coefficient ($\Lambda$), eq. (4), quantifies the relative ease with which fluids move from the matrix blocks to the fracture network; it is typically in the range of $10^{-8} \leq \Lambda \leq 10^{-4}$. It is directly proportional to the ratio of matrix permeability ($k_m$) to fracture permeability ($k_f$). The shape factor $\alpha$ in eq. (4) is a geometry factor that depends on the fracture spacing and the number of fracture families; for three orthogonal families resulting in matrix blocks that are equivalent to spheres with a radius $\rho_m$, we have $\alpha = \frac{15}{\rho_m^2}$[17].

For the definition of the parameters (and corresponding symbols) in eq. (1)-(4) we refer to the nomenclature list.

### 2.2. Response of a rate-controlled harmonic pulse test in a dual-porosity reservoir

The idea behind dual-porosity reservoir models is that two systems overlap spatially and interact through the exchange of fluid [3]. The fracture system loses and gains fluid to and from the matrix. The traditional diffusivity equation (i.e. IARF model) is complemented with a loss term that describes this coupling. An additional equation is required to describe the flow in the matrix blocks. For the restricted model, a simple correlation is introduced between the exchange term and a pressure difference between the fracture and the matrix system. For the unrestricted-flow model, a diffusivity equation is set up in the matrix blocks also, with simplifying assumptions about their shape.

The solution for a HPT starts with the observation that a periodic injection or production rate is a superposition of several harmonic components. Then, the coupled equations are solved for a given driving frequency, and appropriate initial and boundary conditions. The assumption here is that the response to the periodic injection rate is the superposition of the responses to the constituting harmonic components. This is the case if the system response is linear. Both the restricted and the unrestricted case result in a response function in the form of a modified Bessel function of the second kind and zeroth order ($K_0$).

The response function R, which expresses the ratio between pressure response ($p$) to the induced rate disturbance ($q_i$), at a generic distance $r$ from the tested well, is obtained as:

$$R(r) = \frac{p(r)}{q_i} = \frac{1}{2\pi \frac{k}{\mu} H} \frac{K_0(\zeta r)}{\zeta r_w K_1(\zeta r_w)} \tag{5}$$

where parameter $\zeta$ in the Bessel function is a complex number that depends on the frequency and the reservoir characteristics. Moreover, it assumes different values for restricted vs. unrestricted inter-porosity hypothesis:

$$\zeta_{restricted} = \sqrt{\frac{i\omega}{\eta_f} + \frac{i\omega\Lambda(1-\Omega)}{i\omega r_w^2(1-\Omega) + \Omega\Lambda\eta_f}} \tag{6}$$

$$\zeta_{unrestricted} = \sqrt{\frac{i\omega}{\eta_f} + \frac{\Lambda}{5r_w^2}\left[1 - \frac{\sqrt{i\omega\xi}\cos\left(\sqrt{i\omega\xi}\right)}{\sin\left(\sqrt{i\omega\xi}\right)}\right]} \tag{7}$$

$$\eta_f = \frac{\frac{k}{\mu}}{\phi_f c_f}; \xi = \frac{15 r_w^2(\Omega - 1)}{\Omega\Lambda\eta_f} \tag{8}$$

Development details are reported in Appendix A and B, respectively.

In the same way as we have done earlier for single-porosity reservoirs [9], we can incorporate wellbore storage and skin in these solutions. The response function must then be defined for the active well and a possible observer well separately because the skin in the active well does not influence the pressure variation in the observer well. We have:

$$R_w = \frac{p(r_w)}{q_i} = \frac{1}{2\pi \frac{k}{\mu} H} \frac{K_0(\zeta r_w) + S\zeta r_w K_1(\zeta r_w)}{\zeta r_w K_1(\zeta r_w) + C_D\,(\zeta r_w)^2 (S\zeta r_w K_1(\zeta r_w) + K_0(\zeta r_w))} \tag{9}$$

$$R_{obs} = \frac{p(r_{obs})}{q_i} = \frac{1}{2\pi \frac{k}{\mu} H} \frac{K_0(\zeta r_{obs})}{\zeta r_w K_1(\zeta r_w) + C_D(\zeta r_w)^2 (S\zeta r_w K_1(\zeta r_w) + K_0(\zeta r_w))} \tag{10}$$

$$C_D = \frac{C\eta_f}{2\pi \frac{k}{\mu} H r_w^2} \tag{11}$$

Development details are reported in Appendix C.

The response function is a complex number that can be characterized by an amplitude and a phase. The amplitude describes the strength of the response, the phase describes the delay with respect to the driving oscillating flow rate. In addition, we can define the derivative of the response function in a similar way as in pressure transient analysis. We refer to our earlier work for this [9].

### 2.3. Radial composite in dual-porosity reservoir

Determination of a thermal front is particularly important in geothermal reservoir that are often naturally fractured. The temperature in the fracture domain may not be in equilibrium with the temperature in the matrix blocks. As a result, the thermal front can move faster than in single-porosity reservoirs. However, the disequilibrium should be limited to early times [18]. This hypothesis was verified by preliminary numerical simulations.

We have developed response functions under some simplifying hypothesis:

1. The dual-porosity dimensionless parameters do not change with temperature and with the temperature disbalance.
2. The thermal front is approximated by a sharp transition from injection temperature to reservoir temperature.
3. The thermal front variations in time induced by the HPT itself, due to flow and thermal diffusion, are neglected.

4. The vertical variation of the temperature due to the rock temperature gradient is also neglected.

The impact of first and second approximation may be limited since the response to the harmonic stressing is an integration over the complete reservoir – with more weight to pressure disturbances close to the well for higher frequencies, and vice versa.

Concerning the third approximation, the time scale of thermal diffusion is significantly longer than an HPT, which typically last few days; furthermore, water volumes displaced with HPT are expected to be negligible with respect to the water volumes injected before the test take place. Under these conditions, the radial composite assumption based on the initial thermal front state is still acceptable. This was also validated by numerical simulation (section 2.5.3).

The fourth approximation is acceptable if the viscosity variability due to the vertical temperature gradient is significantly less than the one due to the difference between reservoir temperature and injected temperature.

With these conditions, the approach outlined in [12] can be employed. The response functions in the pulser well and in an observation well are provided in Appendix D.

### 2.4. Data processing

To maximize the information provided by harmonic pulse test interpretation, synthetic pressure data were adequately preprocessed by adopting the detrending methodology illustrated in [19] to separate purely periodic components of the signal from non-periodic components. This was particularly important for scenarios where the test started from undisturbed conditions, mimicking a preliminary well shut-in.

Pressure and rate data were then processed according to the data analysis illustrated in [9]. Frequency spectrums of pressure and rate were obtained with FFT (Fast Fourier Transform). Then, frequency peaks, corresponding to harmonic components, were identified. The amplitude ratios and corresponding derivatives vs. frequency were calculated for the selected frequencies and plotted on a log–log plot in the frequency domain, where the frequency components are reported on the abscissae in the form of the associated cycle times, $T = \frac{2\pi}{\omega}$. The dual-porosity with restricted inter-porosity analytical approach (eq. (9) and eq. (6)) was employed to match the data.

Storativity ratio and inter-porosity flow affect derivative trends very similar to what can be observed on the pressure derivative of a conventional well test interpretation for a naturally fractured reservoir. Similarly to the conventional PTA dual-porosity model [17], the inter-porosity flow horizontally shifts the valley, while the storativity ratio regulates the valley amplitude. Storativity ratio and inter-porosity flow influence also the shape of phase shift. However, the influence on phase shift is far less pronounced. As a consequence, amplitude ratio and derivative should drive the match during the HPT analysis in the frequency domain, while phase shift can be used as a further confirmation of the match quality. Similar to a conventional PTA, a step-wise matching procedure is adopted. The first matching parameter is the permeability (k), which is obtained from the derivative stabilization. Then, the storativity ratio and inter-porosity flow have to be adjusted to match the derivative valley. Finally, the skin of the wellbore is adjusted until the amplitude ratio is matched.

### 2.5. Validation scenarios

The presented models (eq. (9) and eq. (D.1)) have been validated against both analytical and numerical models considered as references. Our focus was put on the restricted inter-porosity hypothesis (eq. (6)) since it corresponds to the pseudo-steady state inter-porosity flow model [4] which is the classic and most widely used dual-porosity model [20].

In the following nomenclature "Undisturbed conditions" refers to four scenarios (from S1 to S4) in which HPT is performed from initial static conditions without any interference. "During operation" refers to a scenario (S5) in which the test is performed after a production history from the producing well and while other wells are producing, inducing an aperiodic interfering signal. "Radial composite" considers data generated by a numerical reservoir simulator in the presence of a thermal front (scenario S6).

Properties of the base case scenario (S1) were chosen mimicking a real geothermal fractured reservoir [21]. For Scenario S6, a higher inter-porosity flow coefficient and a higher storativity were assumed in order to enhance the visibility of the cooled zone on the derivative in the frequency domain.

#### 2.5.1. Undisturbed conditions

Four synthetic scenarios (S1-S4) were designed in ideal operational conditions (i.e. no interference and perfect rate switch), spanning different inter-porosity flow coefficients ($\Lambda$) and storativity ratios ($\Omega$), as summarized in Table 1. A reservoir initial pressure of 180 bar and a temperature of 200°C were assumed. Imposed rates and pressure responses are compared in Fig. 2 and Fig. 3.

Synthetic pressure data were generated by the commercial software Saphire from KAPPA engineering. The analytical dual-porosity pseudo-steady state inter-porosity model was adopted [22] and the response of a quartz gauge, with resolution 0.00137895 bar, was generated.

#### 2.5.2. During operations

Scenario S5 represents a test conducted after 90 days of production, during operations: the test is performed on well W1, posed at the center of the domain, while two neighbor wells (W2, W3), 136 m and 176.25 m away respectively (Fig. 4), produce with a non-constant rate (see Fig. 5). Well W1 is characterized by a radius of 0.09144 m and by a mechanical skin S = 2. The aquifer is 50 m thick, with permeability 200 mD and porosity 0.2. Initial pressure is 180 bar.

Synthetic pressure data were obtained by simulation performed with tNavigator® (Rock Flow Dynamics), a high-performance numerical software for reservoir modeling and simulation. The dual-porosity single-permeability model was adopted (DUALPORO option), which assumes that the fluid flow between matrix cells is possible only via fractures, and matrix blocks are not connected to the wellbore [23]. The model considers two grids: the matrix and the fracture. For each grid, the block properties (porosity, permeability, density, compressibility) are defined independently (Table 2). The corresponding parameters for dual-porosity with restricted inter-porosity well test model are $\Omega = 0.01$, $\Lambda = 4*10^{-7}$, (see Appendix E for details); they are reported as Theoretical parameters in Table 6 for comparison with the obtained interpretation results. Imposed water parameters are reported in Table 3.

Notice that the well production before the test does not affect the pressure response regularity, while interference with non-constant production in a neighbor well introduces some aperiodic irregularities, as highlighted in Fig. 5b. Furthermore, the simulated pressure response has a resolution of 0.001 bar, which affects the registered pressure trend: whenever the pressure variation is below the resolution, the pressure trend becomes horizontal.

#### 2.5.3. Radial composite (thermal zone)

Scenario S6 represents a test conducted after 180 days of injection of cold water ($T_{inj} = 20°C$) into an aquifer ($T_{res} = 80°C$) of 300 m thickness. The well is characterized by a radius of 0.09144 m and by a mechanical skin S = 1.

Synthetic pressure data were obtained again by simulation performed with the numerical software tNavigator® with the dual-porosity single-permeability model (DUALPORO option). Matrix and fracture properties (porosity, permeability, density, compressibility, and thermal properties) are reported in Table 4. The corresponding parameters for dual-porosity with restricted inter-porosity well test model are $\Lambda$ =

**Table 1**
Input parameters (dual-porosity restricted inter-porosity model) for the six scenarios.

| Scenario | | S1 | S2 | S3 | S4 | S5 | S6 |
|---|---|---|---|---|---|---|---|
| Match Parameters | Ω(−) | 0.01 | 0.01 | 0.01 | 0.1 | 0.01 | 0.1 |
| | Λ(−) | $4*10^{-7}$ | $4*10^{-8}$ | $4*10^{-6}$ | $4*10^{-7}$ | $4*10^{-7}$ | $6*10^{-7}$ |
| | k(mD) | 200 | 200 | 200 | 200 | 200 | 200 |
| | S(−) | 2 | 2 | 2 | 2 | 2 | 1 |
| Other parameters | $r_w$(m) | 0.09144 | 0.09144 | 0.09144 | 0.09144 | 0.09144 | 0.09144 |
| | $h_{res}$(m) | 300 | 300 | 300 | 300 | 50 | 300 |
| | ϕ(%) | 20 | 20 | 20 | 20 | 20 | 20 |
| | $c_r$($Pa^{-1}$) | $14.5*10^{-10}$ | $14.5*10^{-10}$ | $14.5*10^{-10}$ | $14.5*10^{-10}$ | $14.5*10^{-10}$ | $14.5*10^{-10}$ |
| | $c_w$($Pa^{-1}$) | $7.6*10^{-10}$ | $7.6*10^{-10}$ | $7.6*10^{-10}$ | $7.6*10^{-10}$ | $7.6*10^{-10}$ | $7.6*10^{-10}$ |
| | $\mu_w$ (cP)(res) | 0.177 | 0.177 | 0.177 | 0.177 | 0.177 | 0.376 |
| | $\mu_w$ (cP) (inj) | 0.177 | 0.177 | 0.177 | 0.177 | 0.177 | 0.9 |
| | $B_w$ ($m^3/m^3_{sc}$) | 1.138 | 1.138 | 1.138 | 1.138 | 1.138 | 1.138 |
| | Pi (bar) | 180 | 180 | 180 | 180 | 180 | 180 |

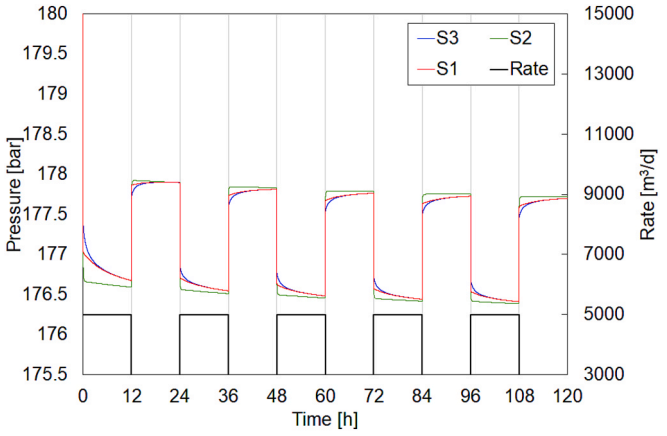


**Fig. 2.** Imposed rate (black) and simulated pressure responses for undisturbed scenarios with different **Λ** (scenarious S1-S3).

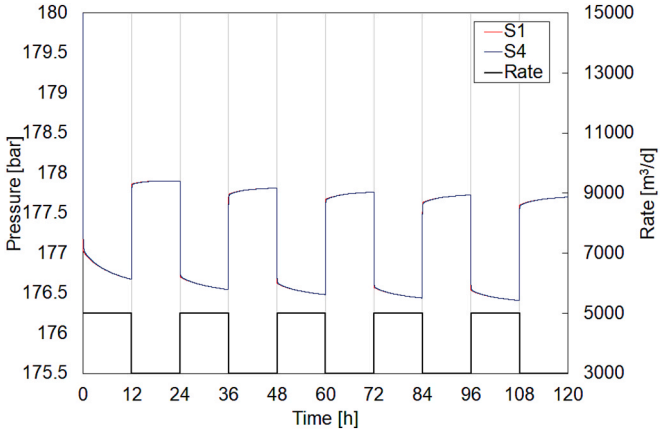


**Fig. 3.** Imposed rate (black) and simulated pressure responses for undisturbed scenarios with different Ω (scenarios S1 vs. S4).

$6*10^{-7}$, Ω = 0.1 (see Appendix E for details); they are reported as Theoretical parameters in Table 7 for comparison with interpretation results. Water properties are reported in Table 5; the imposed variation of water viscosity with temperature is shown in Fig. 6.

The imposed production rate and the obtained pressure profile are shown in Fig. 7. After 180 days of injection, a cooled zone around the well of radius about $r_T$ = 30 m is observed (Fig. 8). The temperature profile is not sharp: it approximates the injection temperature ($T_{inj}$ = 20°C) for about 12 m, then the temperature smoothly increases to 50°C (i.e. midpoint between injected and reservoir temperature) at a distance of about 30 m. The average temperature of this zone is $T_{ave}$ = 29.7°C which corresponds to a viscosity $\mu_{ave}$ = 0.9 cP (Fig. 6).

The proposed analytical interpretation model is not able to reproduce a gradual temperature change. The thermal map was therefore simplified as a radial composite equivalent with two zones (Fig. 8c):

- the outer zone, characterized by reservoir temperature
- the inner zone, corresponding to the cooled zone area around the well delimited by the temperature isotherm T = 50°C (i.e. midpoint between $T_{inj}$ and $T_{res}$), which is characterized by a constant temperature equal to the average temperature of this area ($T_{ave}$ = 29.7°C).

It is pointed out that, due to flow and thermal diffusion, temperature gradients persist throughout the HPT process. However, changes occurred in thermal front during the HPT are negligible (Fig. 8b). Thus, the radial composite assumption based on the temperature distribution observed before the HPT starts is acceptable.

## 3. Results and discussion

A validation of the proposed methodology is provided in the present section. To this end, we have used the output of the previous section as synthetic pressure data, matched them to the theoretical responses by adjusting the model parameters, and compared the results to the known input parameters.

A comparison with classical Pressure Transient Analysis interpretation in time-domain [17] is also provided, to highlight the added value of the proposed methodology. To this end, the pressure data of the first flow period of the HPT was analyzed with the conventional PTA, using the commercial software Saphir. The dual-porosity pseudo-steady state with inter-porosity flow model analytical solution [22] was used for the interpretation.

### 3.1. Undisturbed conditions

The proposed analytical model in the frequency domain correctly reconstructs the synthetic data generated through established solutions for the dual-porosity model in the time domain using the input parameters reported in Table 1 (see Fig. 9 and Fig. 10). In other words, the proposed model allows a good characterization of a fractured reservoir test in terms of permeability, skin, storativity ratio, and inter-porosity flow. As previously said, the phase shift is not very sensitive to the match parameters (Fig. 10). Thus, the match was driven by derivative log–log plot. The match of scenario S3 appears less robust than the S1, S2 and S4 scenarios, because the valley spans the high frequency components, which are generally more affected by noise.

In undisturbed conditions (scenarios S1-S4), a good match can be obtained also with conventional PTA in time with dual-porosity restricted inter-porosity model (Fig. 11). It is pointed out that also

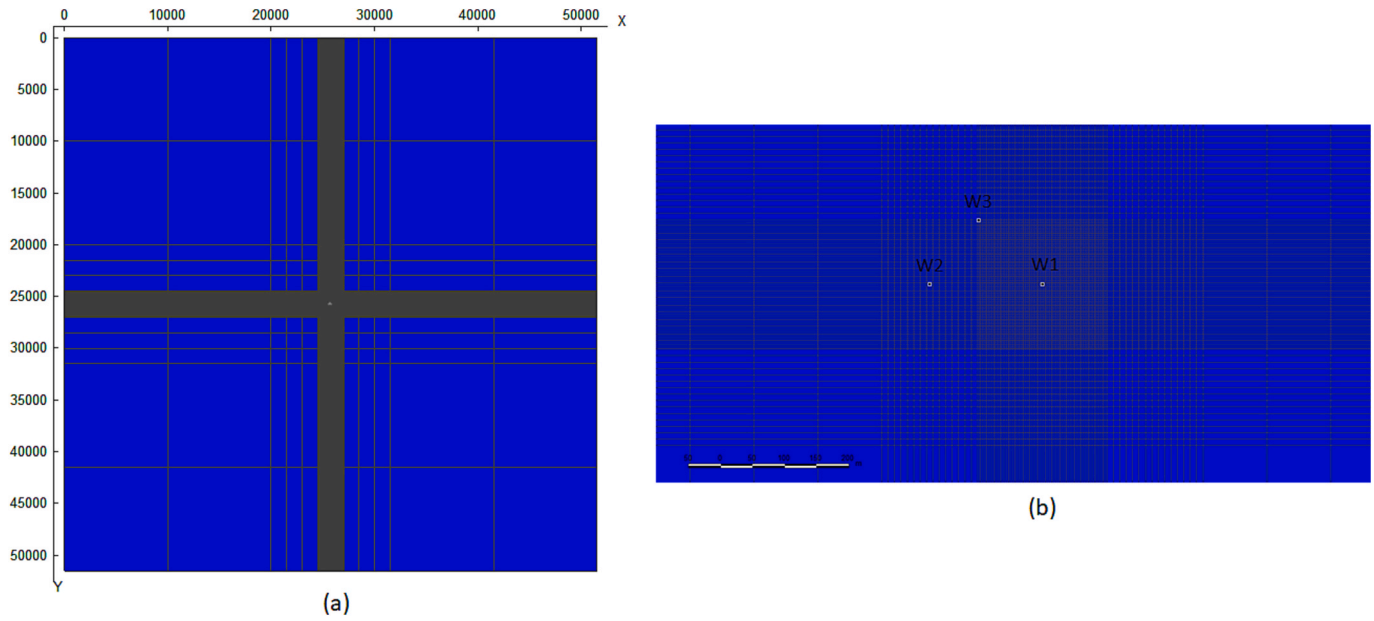


**Fig. 4.** Map of scenario S5: (a) grid of the entire simulation domain; (b) zoom of the central part of the domain, showing the tested well (W1) and interfering wells (W2, W3).

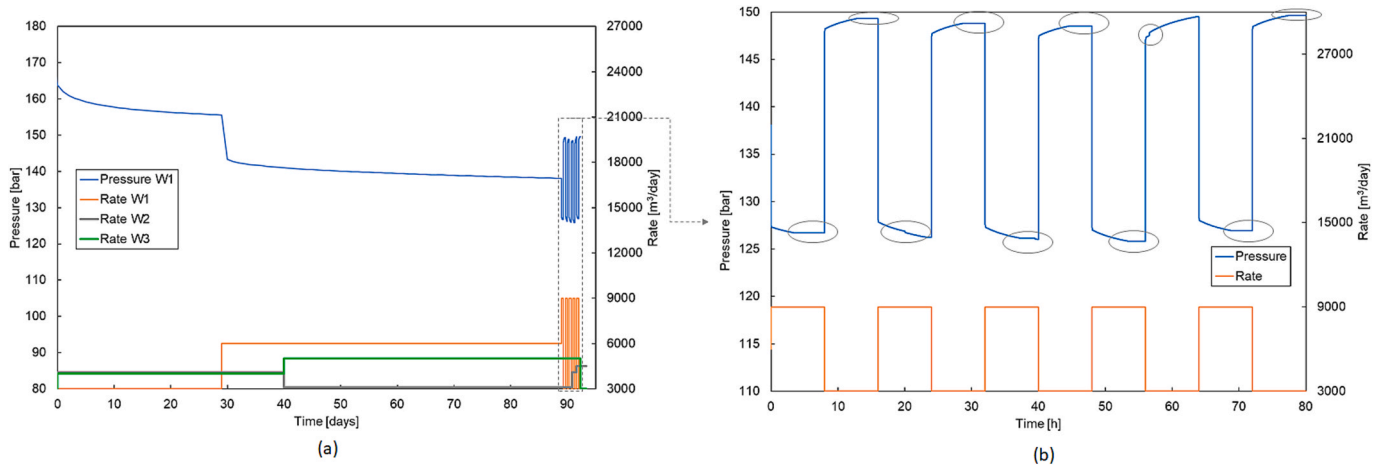


**Fig. 5.** Test in disturbed conditions (scenario S5): (a) imposed rates and simulated pressure response, (b) zoom of the periodic pressure response, where irregularities due to interference rate and pressure variations below pressure resolution are circles.

**Table 2**
Numerical parameters for matrix and fracture part (DUALPORO option) for scenario S5.

| Numerical model parameters | Matrix | Fracture |
|---|---|---|
| Porosity (–) | 0.198 | 0.002 |
| Permeability (mD) | 0.0313 | 200 |
| Density (kg/m3) | 2800 | 2000 |
| Compressibility ($Pa^{-1}$) | $14.5*10^{-10}$ | $14.5*10^{-10}$ |

**Table 3**
Water properties imposed for S5 scenario.

| Water properties | |
|---|---|
| Compressibility ($Pa^{-1}$) | $7.6*10^{-10}$ |
| Viscosity (cP) | 0.177 |
| Volume factor ($m^3/m^3_{sc}$) | 1.138 |

with this approach the interpretation of S3 scenario is more sensitive than the other scenarios. In fact, the matrix recharge, represented by the valley, happens at very short times where, due to the log–log representation, only few points are available.

**Table 4**
Numerical parameters for matrix and fracture part (DUALPORO option) for scenario S6.

| Numerical model parameters | Matrix | Fracture |
|---|---|---|
| Porosity (–) | 0.1968 | 0.032 |
| Permeability (mD) | 0.0471 | 200 |
| Thermal conductivity (kJ/ day/m/ K) | 259.2 | 242 |
| Heat capacity (kJ/kg/K) | 2800 | 1700 |
| Density (kg/m3) | 2800 | 2000 |
| Compressibility ($Pa^{-1}$) | $14.5*10^{-10}$ | $14.5*10^{-10}$ |

### 3.1.1. *Match uncertainty*

Parameters estimated by derivative matching are subject to uncertainty. The degree of uncertainty is influenced by the data quality, and

**Table 5**
Water properties imposed for S6 scenario.

| Water properties | |
|---|---|
| Compressibility ($Pa^{-1}$) | $7.6*10^{-10}$ |
| Viscosity @ Tres (cP) | 0.376 |
| Viscosity @ Tinj (cP) | 1.15 |
| Viscosity @ Tave (cP) | 0.9 |
| Volume factor ($m^3/m^3_{sc}$) | 1.138 |
| Heat capacity (kJ/kg/K) | 4.2 |
| Thermal conductivity (kJ/ day/m/ K) | 57.88 |

mainly depends on pressure gauge resolution and on the precision of rate switching. Influence on permeability and skin estimate was analyzed by the authors in [9] for a IARF model and results are still valid for dual-porosity model. If gauge resolution is good, rate switching is precise and test design is adequate to detect the horizontal stabilization, the permeability and skin interpretation is quite robust. For instance, in S1 a clear stabilization is seen at short periods with HPT approach (Fig. 9a). The PTA interpretation of permeability is also robust, since a clear stabilization is seen and at long times (Fig. 11a). Gauge resolution affects the estimate of inter-porosity flow and storativity parameters more severely, introducing a bit of scattering on the valley in the log–log derivative plot.

Fig. 12 shows the maximum uncertainty range reencountered in scenario S1 for inter-porosity flow and storativity parameters of the dual-porosity model. Similar uncertainty ranges were obtained when interpreting the data with conventional PTA analysis (Fig. 13).

### 3.2. During operations

Three interpretations are provided for scenario S5, one based on the proposed HPT methodology, the other are based on conventional PTA. The HPT interpretation does not require Information about the rates of the interfering wells, as well as any production history prior to the test and the initial pressure. For a fair comparison, the first PTA interpretation assumed that those information were not available, while the second PTA interpretation includes the production history of the tested well only.

Results are compared in Table 6, where theoretical values, corresponding to the imposed numerical parameters, are also reported.

PTA of the first draw down of the test did not yield a good match (Table 6), due to the effect of interfering wells and the previous rate history of the well. Match of the derivative without knowledge of the rate history of the tested well (Fig. 14) gave a significant overestimate of the permeability and an incorrect estimate of the skin (Table 6). Adding the information of previous well history (Fig. 15) improved the permeability estimate, but the match was still incorrect because of well interference (Table 6). The gauge resolution has an additional effect on the PTA derivative, masking the final horizontal stabilization (Fig. 14a).

It is pointed out that some well test interpretation software allow an interpretation with numerical simulation, including interfering wells; however, it would require the knowledge of the entire production history of tested and interfering wells. Furthermore, since numerical simulation is involved in a trial and error tuning of parameters, computational cost would be significantly higher that the presented HPT analytical interpretation in the frequency domain.

Conversely, a good data match was obtained with HPT approach (Table 6). Interference from neighbor wells does not affect the HPT interpretation. In fact, the induced irregularities on the pressure trend are not periodical; thus, they do not affect the periodic components of

**Table 7**
Well test interpretation model parameters (dual-porosity restricted inter-porosity + radial composite) for S6 scenario.

| Scenario | | S6 | | |
|---|---|---|---|---|
| **Parameters** | | **Theoretical values** | **Matched values HPT** | **Matched values PTA** |
| Match Parameters | Ω(−) | 0.1 | 0.1 | 0.1 |
| | Λ(−) | $6*10^{-7}$ | $6.5*10^{-7}$ | $8*10^{-7}$ |
| | k(mD) | 200 | 200 | 200 |
| | S(−) | 1 | 1.7 | 9.3 |
| | $r_{inner}$ (m) | 30 | 30 | – |
| | $\mu_{inner}$(−) | 0.9 | 0.9 | – |
| | Pi (bar) | 180 | – | 180 |
| Other parameters | $r_w$(m) | 0.09144 | | |
| | $h_{res}$(m) | 300 | | |
| | ϕ(%) | 20 | | |
| | $c_t$($Pa^{-1}$) | $2.21*10^{-9}$ | | |
| | $\mu_{outer}$(cP) | 0.376 | | |
| | $B_w$ ($m^3/m^3_{sc}$) | 1.138 | | |

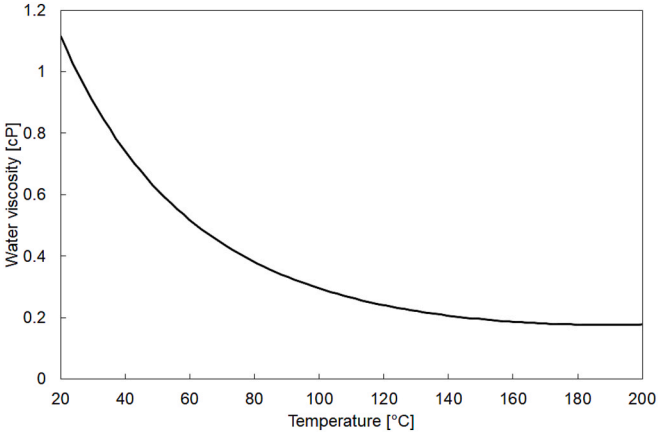


**Fig. 6.** Curve of water viscosity vs. temperature, imposed in the numerical simulator (scenario S6).

**Table 6**
Well test interpretation model parameters (dual-porosity restricted inter-porosity model) for the test conducted during operations (scenario S5).

| Scenario | | S5 | | | |
|---|---|---|---|---|---|
| **Parameters** | | **Theoretical values** | **Matched values HPT** | **Matched values PTA (no history)** | **Matched values PTA (history)** |
| Match Parameters | Ω(−) | 0.01 | 0.012 | 0.0065 | 0.006 |
| | Λ(−) | $4*10^{-7}$ | $4*10^{-7}$ | 1.37e-7 | 3. 8e-7 |
| | k(mD) | 200 | 200 | 369 | 124.5 |
| | S(−) | 2 | 2 | −2.5 | −1.6 |
| | Pi (bar) | 180 | – | 138 | 172.4 |
| Other parameters | $r_w$(m) | 0.09144 | | | |
| | $h_{res}$(m) | 50 | | | |
| | ϕ(%) | 20 | | | |
| | $c_t$($Pa^{-1}$) | $2.21*10^{-9}$ | | | |
| | $\mu_w$ (cP) | 0.177 | | | |
| | $B_w$ ($m^3/m^3_{sc}$) | 1.138 | | | |

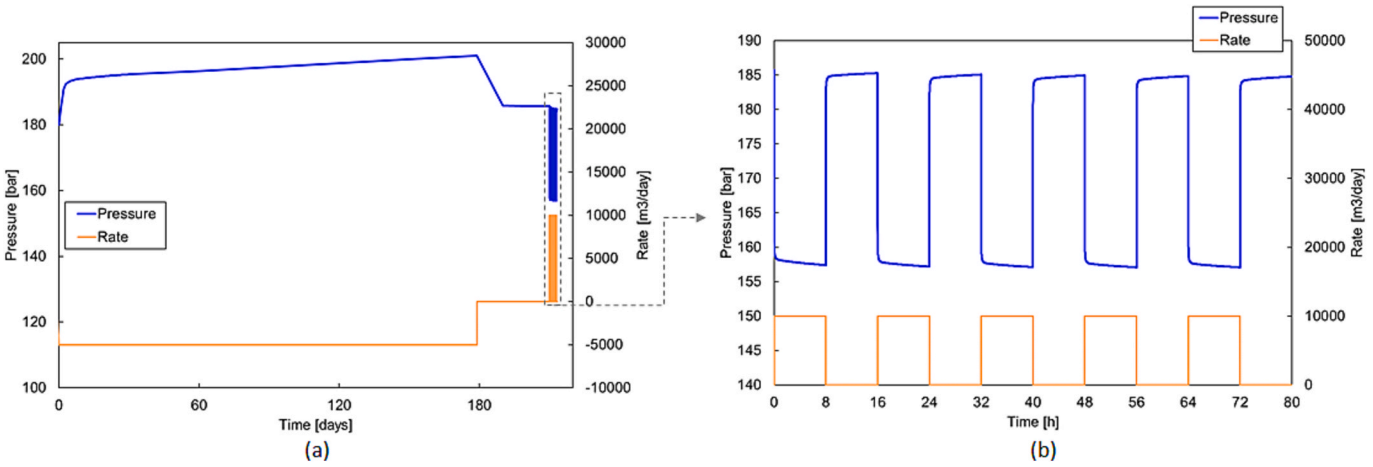


**Fig. 7.** Test with thermal effects (scenario S6): (a) imposed rates and simulated pressure response, (b) zoom of the periodic pressure response.

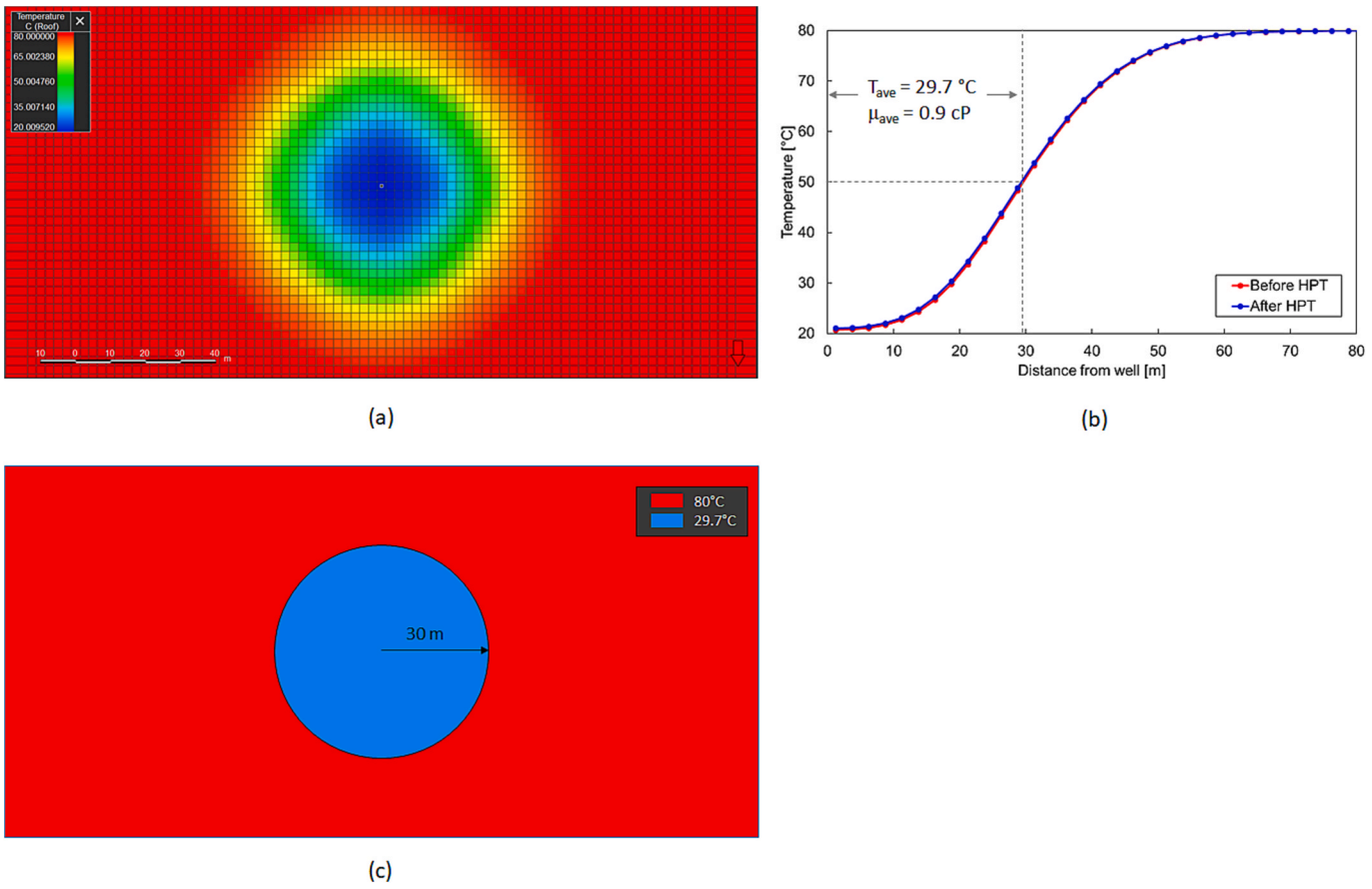


**Fig. 8.** Thermal front after 180 days of injection of cold water: (a) zoom around the well and (b) profile; (c) radial composite equivalent of the zoomed domain.

the pressure spectrum, which are extracted for interpretation. As a result, the effect on the amplitude ratio and derivative is negligible (Fig. 16). The resolution affects the derivative quality at low frequencies ($T \geq 1h$) (Fig. 16), but the data interpretability is not significantly affected.

Since the rates of the interfering wells, as well as the production history before the test are not needed for the HPT interpretation, even in the absence of a preliminary closure of the well, HPT tests can be done during operations, without significant changes in the injection/production plans.

### 3.3. Thermal zone

Two interpretations are provided for scenario S6, which involves the radial composite effect due to the cold-water injection, one based on the proposed HPT methodology and one based on PTA. Matching parameters are compared in Table 7, where theoretical values, corresponding to the imposed numerical parameters, are also reported.

PTA interpretation is shown in Fig. 17b. The joint application of dual-porosity and radial composite models is not allowed in the PTA software: one must choose between either of the two. The derivative could be matched using the dual-porosity model, but this yielded a very

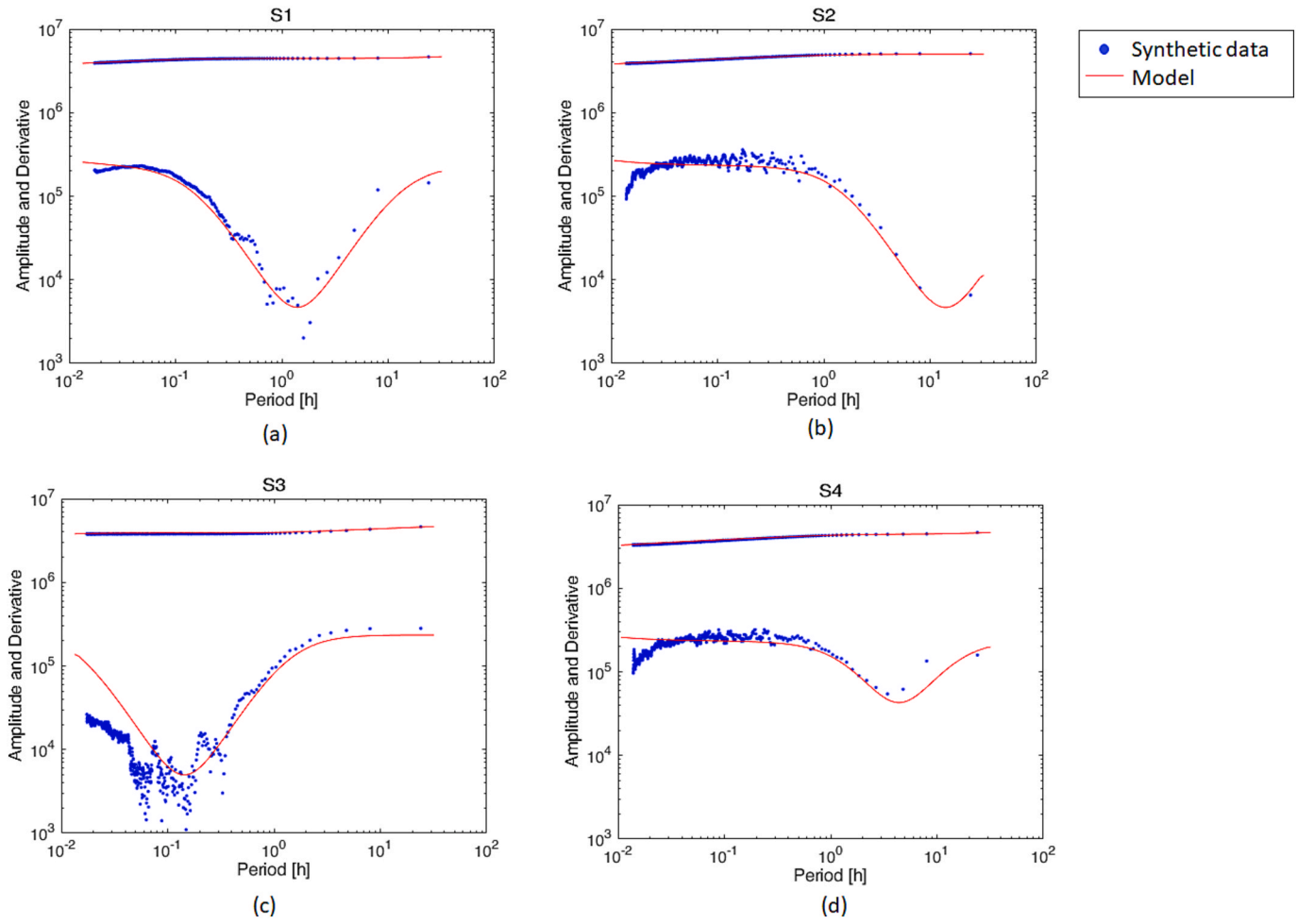


**Fig. 9.** Interpretation in the frequency domain of the HPT data for scenarios S1 to S4. Matching model parameters coincide with imposed input parameters (Table 1).

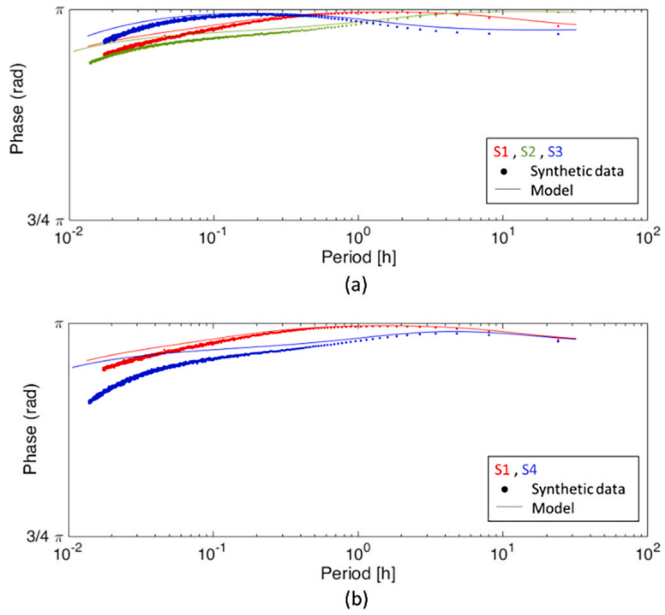


**Fig. 10.** Phase shift in the frequency domain: impact of the scenario and model reconstruction (scenarios S1-S4).

high mechanical skin (S = 9.3), which accounts for the decreased mobility in the cooled zone. A match with the single-porosity radial composite model was not achievable because the stabilization corresponding to the inner zone was completely masked by the valley.

HPT interpretation is shown in Fig. 17a. The first stabilization and the transition to outer zone was visible and a more accurate match of mechanical skin was possible (S = 1.7). The proposed restricted interporosity model in the frequency domain successfully matched both the extension of the cooled zone ($r_{inner}$ = 30 m) and the average temperature of the zone, corresponding to a viscosity of 0.9 cP (Table 7). However, the matching skin was 1.7 instead of 1. The explanation of this mismatch originates from the thermal front not being sharp (Fig. 8b): an artificial additional skin S' =0.7 was needed, corresponding to the inner region ($r_s$ = 15 m) with viscosity $\mu_{inj}$ higher than the average value $\mu_{ave}$:

$$S' = \left(\frac{\mu_{inj}}{\mu_{ave}} - 1\right) ln\left(\frac{r_s}{r_w}\right) \tag{12}$$

It has to be pointed out here that in particular cases the valley in the derivative may overlap with the effect of the thermal boundary, which can complicate its detectability considerably.

### 3.4. Discussion of limitations

While HPT has capabilities complementary to PTA, circumventing some of its limitations, it shares others. In particular, our dual-porosity model is not suitable to represent complex fracture geometries, such as inclined, irregular fractures or those with variable apertures. Further, high-conductivity interconnected fractures, characterized by high flow velocities that could induce Non-Darcy flow in fractures do not fit in the

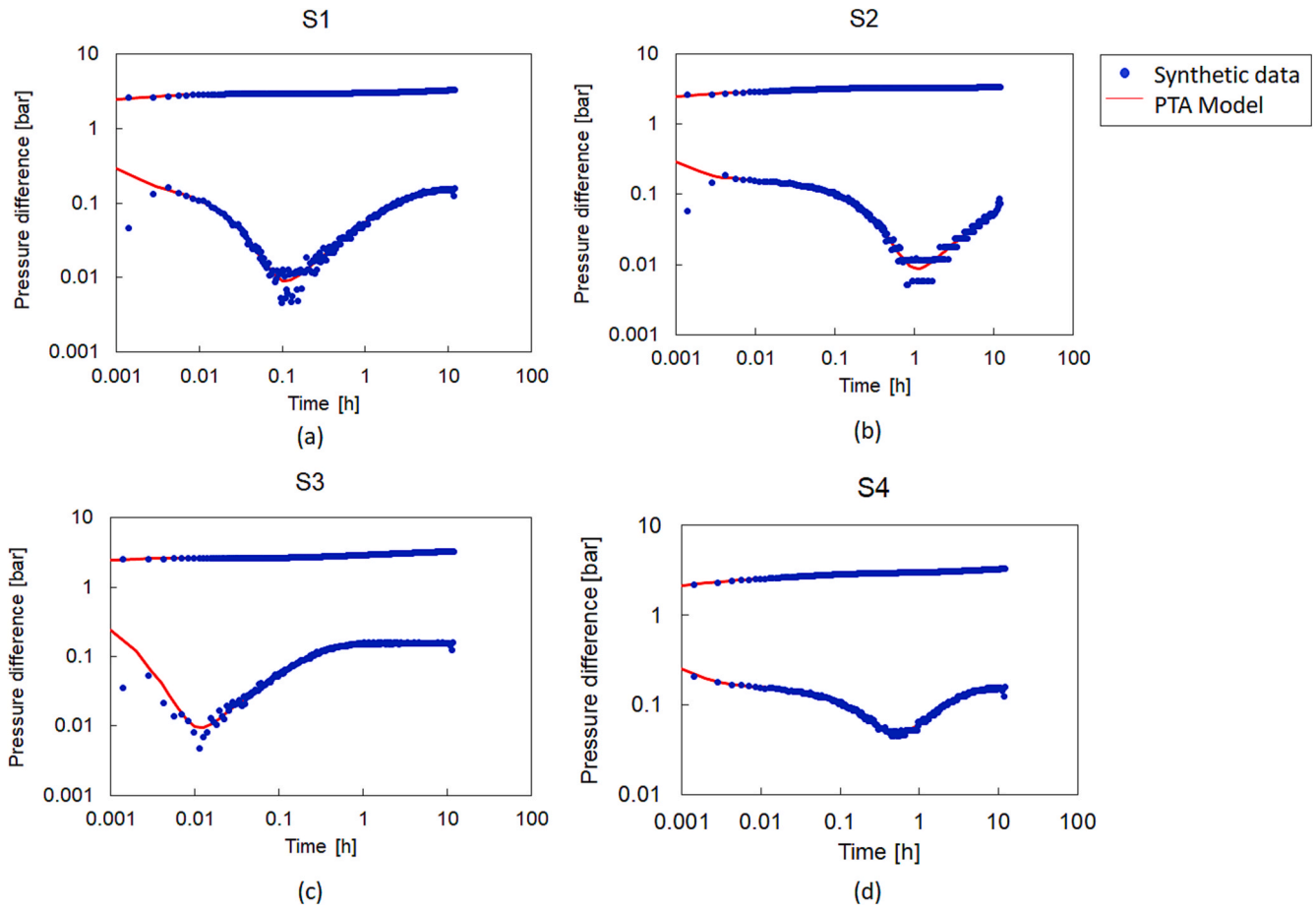


**Fig. 11.** Conventional PTA interpretation of synthetic pressure data for scenarios from S1 to S4. Matching model parameters coincide with imposed input parameters (Table 1).

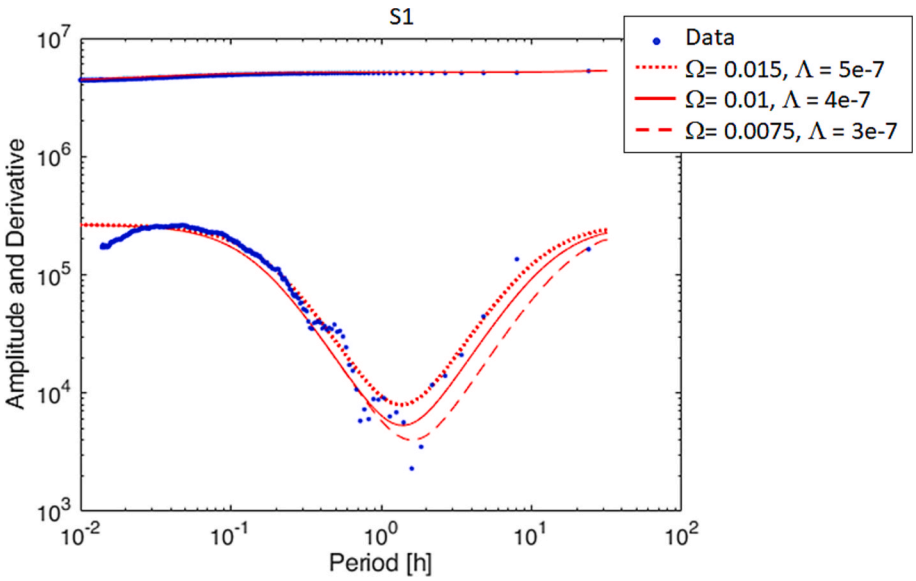


**Fig. 12.** Interpretation in the frequency domain of the HPT data (scenario S1): uncertainty range on the match of inter-porosity and storativity parameters.

theoretical framework, and neither do systems with matrix that exhibits significant variations in permeability and porosity. Nevertheless, naturally fractured reservoir can be usually described as dual-porosity systems [24].

The analytical framework assumes a linear system response, which may not apply in pressure-sensitive formations or in the presence of non-Darcy flow. Still, the HPT methodology could be applicable if the nonlinearity acts on a time scale compatible with the test. For instance, in previous works we successfully applied HPT methodology to a real geothermal reservoir during fracturing operations, where permeability

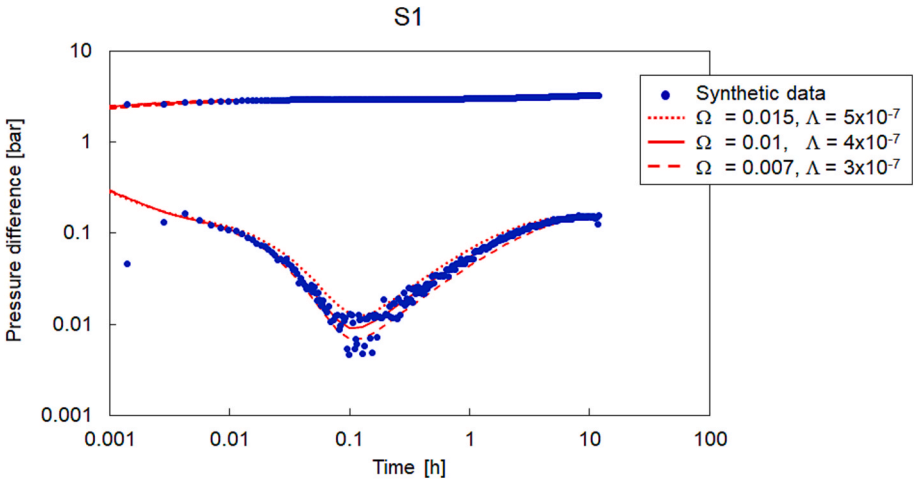


**Fig. 13.** Conventional PTA interpretation of synthetic pressure data for scenario S1: uncertainty range on the match of each parameter.

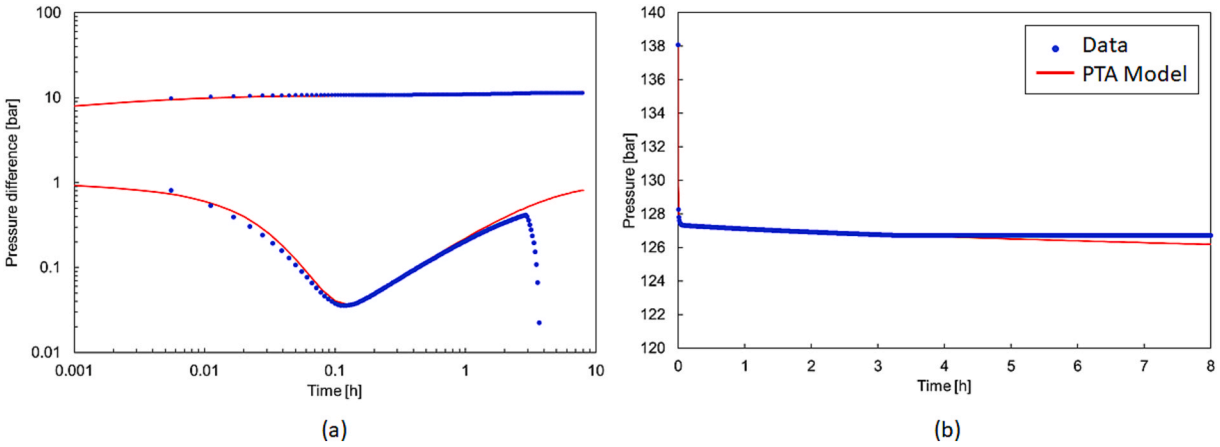


**Fig. 14.** Conventional PTA Interpretation of synthetic pressure data for scenario S5: (a) derivative and (b) pressure reconstruction. No information about interfering well rates and previous rate history were given. Matching parameters are reported in Table 6.

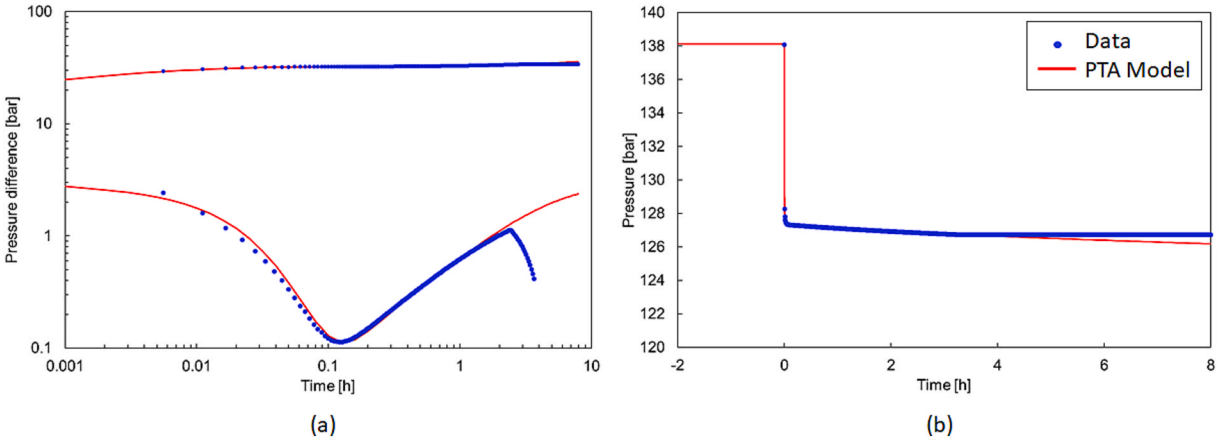


**Fig. 15.** Conventional PTA Interpretation of synthetic pressure data for scenario S5: (a) derivative and (b) pressure reconstruction. Information about previous rate history were given. Matching parameters are reported in Table 6.

changes occurred [10]. In that field test, an HPT was conducted before fracturing for assessing the base permeability; and an HPT of 12 oscillations conducted during fracturing operations was divided in two groups (1–6 and 7–12) which were analyzed separately, in order to show the development of the effective permeability values, and thus the effectiveness of the applied stimulation operations.

We also applied HPT technique to a real gas storage well [11] and estimated the skin associated to the non-Darcy effect. To this end, the HPT was structured with three pulse trains, characterized by the same rate difference but increasing average rate. Each train of pulses was

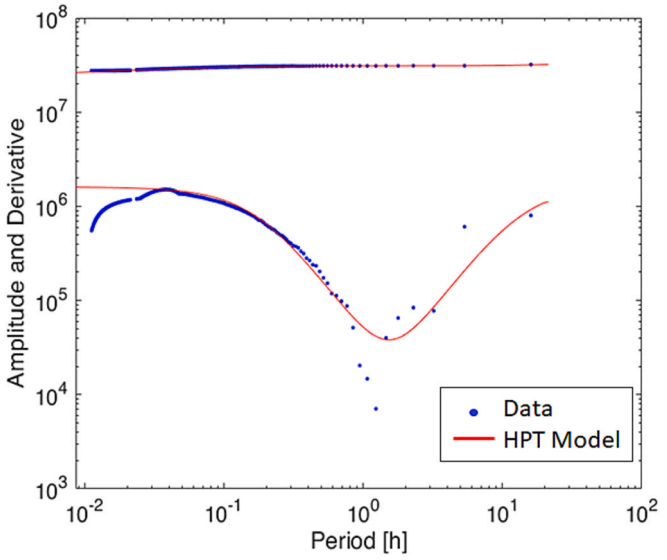


**Fig. 16.** HPT Interpretation of synthetic pressure data for scenario S5, analyzed in the frequency domain. No information about interfering well rates and previous rate history were given. Matching parameters are reported in Table 6.

interpreted separately to get a total skin value; the non-Darcy component of skin was than assessed by interpolating total skin vs. average rate line.

As a final note, we remind that the success of a harmonic pulse test is subject to operational factors [9]:

- A downhole pressure gauge with good resolution
- A precise rate switching (advance or delay < 1% of T)
- A sufficient number of pulses (more than 5)
- A periodicity (T) compatible with the desired investigation distance.

Furthermore, considering that in a dual-porosity case, the valley could mask a significant part of the derivative (e.g. scenario S1 and S3, Fig. 9a, and Fig. 9c), it is extremely important to design a test with a period (T) long enough to allow a robust characterization of reservoir permeability.

## 4. Conclusions

We have devised, implemented, and validated an analytical solution for the characterization of naturally fractured reservoirs through Harmonic Pulse Testing (HPT). The new analytical solutions have been developed in the frequency domain, considering both restricted and unrestricted inter-porosity flow. The solution combines, in terms of both modeling and parameterization, the dual-porosity model, wellbore storage and skin, and the radial composite model —under some simplifying assumptions— to represent the thermal front in naturally fractured geothermal reservoirs.

The restricted inter-porosity model has been validated against both the analytical dual-porosity pseudo-steady-state inter-porosity model and a numerical reservoir simulator capable of representing the thermal front. The reservoir simulator solution is based on the Warren and Root model [18], assuming that fluid flow between matrix cells is possible only via fractures.

Six validation scenarios were analyzed, ranging from simple undisturbed conditions to interference phenomena, thermal effects and ongoing operations.

The validation results demonstrate that HPT is a promising methodology for well-test monitoring in fractured geothermal reservoirs. In particular:

- The proposed model, based on the dual-porosity assumption, correctly reconstructs the pressure/rate amplitude ratio and its derivative in the frequency domain, thus enabling reliable data interpretation and system characterization.
- The model is robust against potential interference from other wells. Therefore, the methodology can be successfully applied during ongoing operations.
- The model allows detection of radial composite effects associated with the presence of a thermal front.

Detecting a thermal front can be challenging in a dual-porosity scenario because the valley characteristic of a dual-porosity derivative may partially or completely overlap with the thermal transition zone, depending on the location of the front. Therefore, careful test design is essential for a successful HPT.

## CRediT authorship contribution statement

**Peter A. Fokker:** Writing – review & editing, Writing – original draft, Software, Methodology, Conceptualization. **Eloisa Salina Borello:** Writing – review & editing, Writing – original draft, Visualization, Validation, Software, Methodology. **Francesca Verga:** Resources, Project administration. **Dario Viberti:** Writing – review & editing, Supervision, Conceptualization.

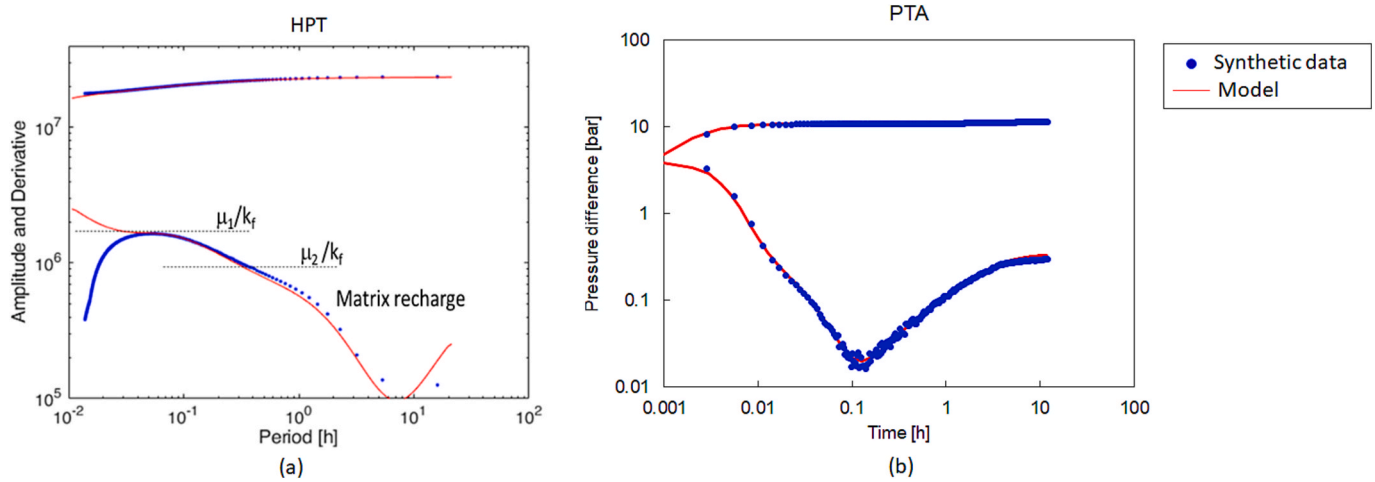


**Fig. 17.** Interpretation of synthetic pressure data for scenario S6: (a) HPT analyzed in the frequency domain; (b) conventional PTA interpretation. Matching parameters are reported in Table 7.

## Declaration of competing interest

The authors declare that they have no known competing financial interests or personal relationships that could have appeared to influence the work reported in this paper.

## Acknowledgments

The authors would like to thank Rock Flow Dynamics for providing support and access to the tNavigator® software used in this work and Kappa Engineering for providing support and access to the Saphir software used in this work.

## Appendix

### A. Dual-porosity with restricted inter-porosity

The fracture system looses and gains fluid to and from the matrix system, signified by a sink $Q_{loss}\left[s^{-1}\right]$ as volume loss rate per unit volume. We have the following differential equation and boundary conditions for the pressure in the fracture system $P(r,t)$[Pa]:

$$\frac{\partial P}{\partial t} = \eta_f \frac{1}{r}\frac{\partial}{\partial r}\left(r\frac{\partial P}{\partial r}\right) - \frac{1}{\phi_f c_f} Q_{loss}(r,t) \tag{A.1}$$

$$\left[\frac{\partial P}{\partial r}\right]_{r=r_w} = \frac{-1}{2\pi r_w \frac{k}{\mu} H} Q_i(t) \tag{A.2}$$

$$P(r\to\infty) = 0 \tag{A.3}$$

$$\eta_f = \frac{\frac{k}{\mu}}{\phi_f c_f} \tag{A.4}$$

The fractures are coupled to the matrix system. The restricted inter-porosity system is based on the work of Warren and Root [4] and assumes an average pressure in the matrix blocks that drives the communication with the fracture system. We use three fracture families; this results in the geometry factor $\alpha = \frac{15}{\rho_m^2}$ in which a 3D radially symmetric sphere with radius $\rho_m[m]$ is introduced [17]. We obtain for the pressure $P_m(\rho,t)$[Pa] in the matrix and the boundary conditions, at the local coordinate system in the matrix indicated with $\rho$:

$$Q_{loss}(r,t) = \alpha \frac{k_m}{\mu}(P - P_m) \tag{A.5}$$

$$\phi_m c_m \frac{\partial P_m}{\partial t} = \alpha \frac{k_m}{\mu}(P - P_m) \tag{A.6}$$

$$\alpha = \frac{15}{\rho_m^2} \tag{A.7}$$

Now we introduce a harmonic time variation of pressures and rates, with $\omega$ the angular frequency:

$$P(r,t) = p(r)e^{i\omega t} \tag{A.8}$$

$$Q_i(t) = q_i e^{i\omega t} \tag{A.9}$$

$$Q_{loss}(r,t) = q_{loss}(r)e^{i\omega t} \tag{A.10}$$

$$P_m(\rho,t) = p_m(\rho)e^{i\omega t} \tag{A.11}$$

And we obtain:

$$i\omega p = \eta_f \frac{1}{r}\frac{d}{dr}\left(r\frac{dp}{dr}\right) - \frac{1}{\phi_f c_f} q_{loss}(r) \tag{A.12}$$

$$\left[\frac{dp}{dr}\right]_{r=r_w} = \frac{-1}{2\pi r_w \frac{k}{\mu} H} q_i \tag{A.13}$$

$$p(r\to\infty) = 0 \tag{A.14}$$

$$q_{loss}(r) = \alpha \frac{k_m}{\mu}(p - p_m) \tag{A.15}$$

$$i\omega\phi_m c_m p_m = \alpha \frac{k_m}{\mu}(p - p_m) \tag{A.16}$$

$$p_m = \frac{\alpha \frac{k_m}{\mu}}{i\omega\phi_m c_m + \alpha \frac{k_m}{\mu}} p \tag{A.17}$$

The last equation (A.17) gives the delay and amplitude reduction of the pressure in the matrix blocks with respect to the pressure in the fracture

system. Inserting this into the expressions for the loss rate and the differential equation of the pressure in the fracture system results in the modified Bessel function for the pressure:

$$\frac{1}{r}\frac{d}{dr}\left(r\frac{dp}{dr}\right) = p\frac{i\omega}{\frac{k}{\mu}}\left[\phi_f c_f + \frac{\alpha\frac{k_m}{\mu}\phi_m c_m}{i\omega\phi_m c_m + \alpha\frac{k_m}{\mu}}\right] \tag{A.18}$$

We obtain the solution for the response function with respect to the injection rate:

$$R = \frac{p(r)}{q_i} = \frac{1}{2\pi\frac{k}{\mu}H}\frac{K_0(\zeta_f r)}{\zeta_f r_w K_1(\zeta_f r_w)} \tag{A.19}$$

$$\zeta_f = \sqrt{\frac{i\omega}{\frac{k}{\mu}}\left(\phi_f c_f + \frac{\alpha\frac{k_m}{\mu}\phi_m c_m}{i\omega\phi_m c_m + \alpha\frac{k_m}{\mu}}\right)} = \sqrt{\frac{i\omega}{\eta_f}\left(1 + \frac{\eta_f\Lambda(1-\Omega)}{i\omega r_w^2(1-\Omega) + \Omega\Lambda\eta_f}\right)} \tag{A.20}$$

*B. Dual-porosity with unrestricted inter-porosity*

We consider a well in a 2D radially symmetric fracture system. The fracture system looses fluid to the matrix system, signified by a sink $Q_{loss}\left[\mathrm{s}^{-1}\right]$ as volume loss rate per unit volume. When we further define fracture porosity $\phi_f[-]$; total compressibility in the fracture system $c_f\left[\mathrm{Pa}^{-1}\right]$, and well injection rate per well unit length $Q_i(t)\left[\mathrm{m}^2\mathrm{s}^{-1}\right]$, we have the following differential equation and boundary conditions for the pressure in the fracture system $P(r,t)$[Pa] (we define the well radius $r_w[m]$, permeability $k\left[m^2\right]$ and viscosity $\mu$[Pa.s]):

$$\frac{\partial P}{\partial t} = \eta_f\frac{1}{r}\frac{\partial}{\partial r}\left(r\frac{\partial P}{\partial r}\right) - \frac{1}{\phi_f c_f}Q_{loss}(r,t) \tag{B.1}$$

$$\left[\frac{\partial P}{\partial r}\right]_{r=r_w} = \frac{-1}{2\pi r_w\frac{k}{\mu}H}Q_i(t) \tag{B.2}$$

$$P(r\to\infty) = 0 \tag{B.3}$$

$$\eta_f = \frac{\frac{k}{\mu}}{\phi_f c_f} \tag{B.4}$$

The fractures are coupled to the matrix system; we approximate a block with a 3D radially symmetric sphere with radius $\rho_m[m]$. With the matrix porosity $\phi_m[-]$, the total compressibility in the matrix blocks $c_m\left[\mathrm{Pa}^{-1}\right]$, the permeability in the matrix $k_m[\mathrm{m}^2]$, and assuming that the flux at the sphere boundary is $Q_{lin} = Q_{loss}\frac{\frac{4}{3}\rho_m^3}{4\pi\rho_m^2} = Q_{loss}\frac{\rho_m}{3}$, we obtain for the pressure $P_m(\rho,t)$[Pa] in the matrix and the boundary conditions, at the local coordinate system in the matrix indicated with $\rho$:

$$\frac{\partial P_m}{\partial t} = \eta_m\frac{1}{\rho^2}\frac{\partial}{\partial\rho}\left(\rho^2\frac{\partial P_m}{\partial\rho}\right) \tag{B.5}$$

$$\left[\frac{\partial P_m}{\partial\rho}\right]_{\rho=\rho_m} = \frac{\rho_b}{3\frac{k_m}{\mu}}Q_{loss}(r,t) \tag{B.6}$$

$$P_m(\rho_m,t) = P(r,t) \tag{B.7}$$

$$\eta_m = \frac{\frac{k_m}{\mu}}{\phi_m c_m} \tag{B.8}$$

Now we introduce a harmonic time variation of pressures and rates, with $\omega$ the angular frequency:

$$P(r,t) = p(r)e^{i\omega t} \tag{B.9}$$

$$Q_i(t) = q_i e^{i\omega t} \tag{B.10}$$

$$Q_{loss}(r,t) = q_{loss}(r)e^{i\omega t} \tag{B.11}$$

$$P_m(\rho,t) = p_m(\rho)e^{i\omega t} \tag{B.12}$$

And we obtain:

$$i\omega p = \eta_f\frac{1}{r}\frac{d}{dr}\left(r\frac{dp}{dr}\right) - \frac{1}{\phi_f c_f}q_{loss}(r) \tag{B.13}$$

$$\left[\frac{dp}{dr}\right]_{r=r_w} = \frac{-1}{2\pi r_w \frac{k}{\mu} H} q_i \tag{B.14}$$

$$p(r \to \infty) = 0 \tag{B.15}$$

$$\frac{1}{\rho^2}\frac{d}{d\rho}\left(\rho^2 \frac{dp_m}{d\rho}\right) = \frac{i\omega}{\eta_m} p_m \tag{B.16}$$

$$q_{loss}(r) = 3\frac{k_m}{\mu}\frac{1}{\rho_b}\left[\frac{dp_m}{d\rho}\right]_{\rho=\rho_m} \tag{B.17}$$

$$p_m(\rho_m) = p(r) \tag{B.18}$$

The solution in the matrix system is a spherical Bessel function. Combining the general solution with the boundary conditions, and requiring finite solution values at $\rho = 0$, we have:

$$\frac{p_m(\rho)}{p(r)} = \frac{\rho_m}{\sin(\zeta_m \rho_m)}\frac{\sin(\zeta_m \rho)}{\rho} \tag{B.19}$$

$$\zeta_m = \sqrt{\frac{-i\omega}{\eta_m}} \tag{B.20}$$

The loss function then becomes:

$$q_{loss}(r) = p(r)\frac{k_m}{\mu}\frac{3}{\rho_m^2}\left(\frac{\zeta_m \rho_m \cos(\zeta_m \rho_m)}{\sin(\zeta_m \rho_m)} - 1\right) = p(r)\frac{k_m}{\mu}\frac{3}{\rho_m^2}\left(\frac{\sqrt{i\omega\xi}\cos\left(\sqrt{i\omega\xi}\right)}{\sin\left(\sqrt{i\omega\xi}\right)} - 1\right) \tag{B.21}$$

$$\xi = \frac{15 r_w^2 (\Omega - 1)}{\Omega \Lambda \eta_f} \tag{B.22}$$

Inserting this into eq. (B.13), with the conditions (B.14) and (B.15), we obtain a modified Bessel equation and its solution:

$$\frac{1}{r}\frac{d}{dr}\left(r\frac{dp}{dr}\right) = p\left(\frac{i\omega}{\eta_f} + \frac{3k_m}{k\rho_m^2}\left[1 - \frac{\sqrt{i\omega\xi}\cos\left(\sqrt{i\omega\xi}\right)}{\sin\left(\sqrt{i\omega\xi}\right)}\right]\right) \tag{B.23}$$

$$R = \frac{p(r)}{q_i} = \frac{1}{2\pi\frac{k}{\mu}H} \bullet \frac{K_0(\zeta_f r)}{\zeta_f r_w K_1(\zeta_f r_w)} \tag{B.24}$$

$$\zeta_f = \sqrt{\frac{i\omega}{\eta_f} + \frac{\Lambda}{5r_w^2}\left[1 - \frac{\sqrt{i\omega\xi}\cos\left(\sqrt{i\omega\xi}\right)}{\sin\left(\sqrt{i\omega\xi}\right)}\right]} \tag{B.25}$$

### C. Incorporation of wellbore storage and skin

Wellbore storage and skin can be incorporated in the same way as was done for the Infinite Acting Radial Flow (IARF) solution [9]; and we get for both cases ($\zeta = \zeta_f$ or $\zeta = \zeta_{fl}$ respectively for the restricted and unrestricted cases) in the pulser well and in an observer well:

$$R = \frac{p(r_w)}{q_i} = \frac{1}{2\pi\frac{k}{\mu}H}\frac{K_0(\zeta r_w) + S\zeta r_w K_1(\zeta r_w)}{\zeta r_w K_1(\zeta r_w) + C_D(\zeta r_w)^2 (S\zeta r_w K_1(\zeta r_w) + K_0(\zeta r_w))} \tag{C.1}$$

$$R_{obs} = \frac{p(r_{obs})}{q_i} = \frac{1}{2\pi\frac{k}{\mu}H}\frac{K_0(\zeta r_{obs})}{\zeta r_w K_1(\zeta r_w) + C_D(\zeta r_w)^2 (S\zeta r_w K_1(\zeta r_w) + K_0(\zeta r_w))} \tag{C.2}$$

$$C_D = \frac{C\eta_f}{2\pi\frac{k}{\mu}Hr_w^2} \tag{C.3}$$

### D. Incorporation of a temperature boundary

We simplify the system with two assumptions. The first is that the dual-porosity dimensionless parameters do not change with temperature and with the temperature disbalance. The second is that the thermal front is a sharp transition from injection temperature to reservoir temperature. Under these conditions, we may argue in an analogous way as in [12]. The response in the well is complemented with the effect of the skin. In an observation well, the response depends on whether the position is inside or outside the thermal boundary ($j = 1, 2$ inside and outside the affected area). The solution in the outer zone does not contain the term with the Bessel function of the first kind since it must vanish for large distances.

$$R = C_{1K}K_0(\zeta_1 r_w) + C_{1I}I_0(\zeta_1 r_w) + S\zeta_1 r_w[C_{1K}K_1(\zeta_1 r_w) - C_{1I}I_1(\zeta_1 r_w)] \tag{D.1}$$

$$R_{obs} = \begin{cases} C_{1K}K_0(\zeta_1 r_{obs}) + C_{1I}I_0(\zeta_1 r_w) & (r_{obs} < r_{thermal}) \\ C_{2K}K_0(\zeta_2 r_{obs}) & (r_{obs} \geq r_{thermal}) \end{cases} \tag{D.2}$$

$$\zeta^j_{restricted} = \sqrt{\frac{i\omega}{\eta_{f,j}} + \frac{i\omega\Lambda(1-\Omega)}{i\omega r_w^2(1-\Omega) + \Omega\Lambda\eta_{f,j}}} \tag{D.3}$$

$$\zeta^j_{unrestricted} = \sqrt{\frac{i\omega}{\eta_{f,j}} + \frac{\Lambda}{5r_w^2}\left[1 - \frac{\sqrt{i\omega\xi}\cos\left(\sqrt{i\omega\xi}\right)}{\sin\left(\sqrt{i\omega\xi}\right)}\right]} \tag{D.4}$$

$$\eta_{f,j} = \frac{\frac{k}{\mu_j}}{\phi_f c_f}; \xi_j = \frac{15r_w^2(\Omega-1)}{\Omega\Lambda\eta_{f,j}} \tag{D.5}$$

The parameters $C_{1K}$, $C_{1I}$ and $C_{2K}$ need to be determined by the boundary and interface conditions: continuity of the pressure at the interface; continuity of flow at the interface, and the imposed flow rate with incorporation of wellbore storage at the wellbore. We have:

$$A\begin{pmatrix} C_{1k} \\ C_{1I} \\ C_{2K} \end{pmatrix} = \begin{pmatrix} 0 \\ 0 \\ 1 \end{pmatrix} \tag{D.6}$$

$$A = \begin{pmatrix} i\omega C_D k_{001} + (2\pi H\lambda_1 + i\omega CS)k_{101} & i\omega C i_{001} - (2\pi H\lambda_1 + i\omega CS)i_{101} & 0 \\ k_{011} & i_{011} & -k_{012} \\ -\lambda_1 k_{111} & \lambda_1 i_{111} & \lambda_2 i_{112} \end{pmatrix}$$

$$\begin{array}{lll} k_{001} = K_0(\zeta_1 r_w) & k_{011} = K_0(\zeta_1 r_1) & k_{012} = K_0(\zeta_2 r_1) \\ k_{101} = \zeta_1 r_w K_1(\zeta_1 r_w) & k_{111} = \zeta_1 r_1 K_1(\zeta_1 r_1) & k_{112} = \zeta_2 r_1 K_1(\zeta_2 r_1) \end{array} \tag{D.7}$$

$$\begin{array}{ll} i_{001} = I_0(\zeta_1 r_w) & i_{011} = I_0(\zeta_1 r_1) \\ i_{101} = \zeta_1 r_w I_1(\zeta_1 r_w) & i_{111} = \zeta_1 r_1 I_1(\zeta_1 r_1) \end{array}$$

### *E. From dual-porosity simulator to well-test parameters*

Porosity and permeability of matrix and fracture components of the numerical dual-porosity model can be expressed in function of the dimensionless parameters storativity ratio (Ω), eq. (3), and inter-porosity flow coefficient (Λ), eq. (4).

The permeabilities have been defined with respect to the gross volume [17]. Therefore, because the flow between blocks is only handled by the fracture system, $k_f = k$. Combined with the definition of the inter-porosity flow coefficient (eq. (4)), we then have:

$$k_f = k \tag{E.1}$$

$$k_m = \frac{\Lambda}{\alpha r_w^2}k \tag{E.2}$$

Assuming three orthogonal families of fractures resulting in matrix blocks that are equivalent to spheres with a radius$\rho_m = 7$ m, the shape factor becomes $\alpha = \frac{15}{\rho_m{}^2} = 0.3061$.

For the porosity of the matrix and the fracture system, we use eqs. (1) and (3) to obtain:

$$\phi_f = \frac{\phi c_m \Omega}{c_f(1-\Omega) + c_m\Omega} = \frac{\Omega\phi}{\Omega + (1-\Omega)\frac{c_f}{c_m}} = \phi\frac{1}{1 + \frac{c_f}{c_m}\frac{1-\Omega}{\Omega}} \tag{E.3}$$

$$\phi_m = \phi\frac{1}{1 + \frac{c_m}{c_f}\frac{\Omega}{1-\Omega}} \tag{E.4}$$

## Data availability

Research data is available at https://github.com/REDD-PoliTO/HPT-data-.

## References


[1] Grant MA, Bixley PF. *Geothermal reservoir engineering*. 2nd ed. Burlington, MA: Academic Press; 2015.

[2] Gringarten AC. From straight lines to deconvolution: the evolution of the state of the art in well test analysis. SPE Reserv Eval Eng 2008;11(1):41–62. https://doi.org/10.2118/102079-PA.

[3] Bourdet D. *Well test analysis: the use of advanced interpretation models*, 1st ed. in Handbook of petroleum exploration and production 1567-8032, no. 3. Amsterdam Boston: Elsevier, 2010.

[4] Warren JE, Root PJ. The behavior of naturally fractured reservoirs. Soc Pet Eng J Sept. 1963;3(03):245–55. https://doi.org/10.2118/426-PA.

[5] Peng S, Zhang J. Stress-dependent permeability, in *Engineering Geology for Underground Rocks*, Berlin, Heidelberg: Springer Berlin Heidelberg, 2007, pp. 199–220. doi: 10.1007/978-3-540-73295-2_8.

[6] Johnson RA, Greenkorn CR, Woods EG. Pulse testing: a new method for describing reservoir flow properties between wells. J Pet Tech 1966;18(12):1599–604. https://doi.org/10.2118/1517-PA.

[7] Hollaender F, Filas JG, Bennett CO, Gringarten AC. Use of downhole production/reinjection for zero-emission well testing: challenges and rewards, in *Proceedings - SPE Annual Technical Conference and Exhibition*, San Antonio, TX, 2002, pp. 2443–2452. doi: 10.2118/77620-MS.

[8] Cardiff M, Barrash W. Analytical and semi-analytical tools for the design of oscillatory pumping tests. Groundwater Nov. 2015;53(6):896–907. https://doi.org/10.1111/gwat.12308.
[9] Fokker PA, Salina Borello E, Verga F, Viberti D. Harmonic pulse testing for well performance monitoring. J Petrol Sci Eng 2018;162:446–59. https://doi.org/10.1016/j.petrol.2017.12.053.
[10] Salina Borello E *et al.*, Harmonic pulse testing for well monitoring: application to a fractured geothermal reservoir, *Water Resour Res*, vol. 55, no. 6, pp. 4727–4744, June 2019, doi: 10.1029/2018WR024029.
[11] Salina Borello E, Fokker PA, D. Viberti, R. Espinoza, and F. Verga, Harmonic-pulse testing for non-Darcy-effects identification, *SPE Reservoir Evaluation & Engineering*, vol. 20, no. 2, pp. 486–501, 2017, doi: 10.2118/183649-PA.
[12] Fokker PA, E. Salina Borello, D. Viberti, F. Verga, and J.-D. Van Wees, Pulse testing for monitoring the thermal front in aquifer thermal energy storage, *Geothermics*, vol. 89, p. 101942, Jan. 2021, doi: 10.1016/j.geothermics.2020.101942.
[13] Cheng Y, Renner J. Exploratory use of periodic pumping tests for hydraulic characterization of faults. Geophys J Int Jan. 2018;212(1):543–65. https://doi.org/10.1093/gji/ggx390.
[14] Hofmann H, et al. First field application of cyclic soft stimulation at the Pohang Enhanced Geothermal System site in Korea. Geophys J Int May 2019;217(2):926–49. https://doi.org/10.1093/gji/ggz058.
[15] Fokker PA, Salina Borello E, Serazio C, Verga F. Estimating reservoir heterogeneities from pulse testing. J Petrol Sci Eng 2012;86–87:15–26. https://doi.org/10.1016/j.petrol.2012.03.017.
[16] Patterson JR, Cardiff M. Stiff, smooth, and solid? complex fracture hydraulics' imprint on oscillatory hydraulic testing, *Water Resour Res*, vol. 59, no. 11, p. e2023WR034621, Nov. 2023, doi: 10.1029/2023WR034621.
[17] Bourdet D. *Well Test Analysis: The Use of Advanced Interpretation Models: Handbook of Petroleum Exploration and Production, 3*. Elsevier Science, 2002. [Online]. Available: https://www.amazon.com/Well-Test-Analysis-Interpretation-Exploration/dp/0444549889?SubscriptionId=0JYN1NVW651KCA56C102&tag=techkie-20&linkCode=xm2&camp=2025&creative=165953&creativeASIN=0444549889.
[18] Bodvarsson GS, Tsang C-F. Injection Into A Fractured Geothermal Reservoir, presented at the Geothermal Resource Council, in LBL Publications. Soult Lake City (UT): Lawrence Berkeley National Laboratory, 1980. [Online]. Available: https://escholarship.org/uc/item/19j6b2xz.
[19] Viberti D, E. Salina Borello, and F. Verga, Pressure detrending in harmonic pulse test interpretation: when, why and how, *Energies*, vol. 11, no. 6, 2018, doi: 10.3390/en11061540.
[20] He Y, Chen X, Zhang Y, Yu W. Modeling inter-porosity flow functions and shape factors in low-permeability naturally fractured reservoir. J Petrol Sci Eng July 2017;156:110–7. https://doi.org/10.1016/j.petrol.2017.05.006.
[21] Aydin H, Merey S, Akin S. Pressure Transient Analysis of Alaşehir Geothermal Reservoir. Presented at the Stanford Geothermal Workshop. 2024.
[22] Houze O, D. Viturat, O. S. Fjaere, and et al., *Dynamic Data Analysis*, V5.20. Kappa Engineering; 2018.
[23] Reservoir Simulator tNavigator (version 4.2). User Manual." RFDynamics, 2004-2016, 2024.
[24] Kazemi H, Merrill LS, Porterfield KL, Zeman PR. Numerical simulation of water-oil flow in naturally fractured reservoirs. Soc Pet Eng J Dec. 1976;16(06):317–26. https://doi.org/10.2118/5719-PA.